Electronic structure of $Cr_{1-\delta}X(X=S,Te)$ studied by Cr 2*p* soft x-ray magnetic circular dichroism

Koichiro Yaji, Akio Kimura,* Chiyuki Hirai, and Masaki Taniguchi
Graduate School of Science, Hiroshima University, 1-3-1 Kagamiyama, Higashi-Hiroshima 739-8526, Japan

Michie Koyama
Kure National College of Technology, Agaminami 2-2-11, Kure 737, Japan

Hitoshi Sato and Kenya Shimada
Hiroshima Synchrotron Radiation Center, Hiroshima University, 2-313 Kagamiyama, Higashi-Hiroshima 739-8526, Japan

Arata Tanaka
Department of Quantum Matter, ADSM, Hiroshima University, 1-3-1 Kagamiyama, Higashi-Hiroshima 739-8526, Japan

Takayuki Muro
Japan Synchrotron Radiation Research Institute, Mikazuki, Hyogo 679-5143, Japan

Shin Imada and Shigemasa Suga
Graduate School of Engineering Science, Osaka University, 1-3 Machikaneyama, Toyonaka, Osaka 560-8531, Japan
(Received 5 March 2004; published 5 August 2004)

Cr 2*p* core excited x-ray absorption and x-ray magnetic circular dichroism (XMCD) spectra of ferromagnetic $Cr_{1-\delta}Te$ with several concentrations of $\delta=0.11-0.33$ and ferrimagnetic Cr_5S_6 have been measured. The observed XMCD line shapes are found to very weakly depend on δ for $Cr_{1-\delta}Te$. The experimental results are analyzed by means of a configuration-interaction cluster model calculation with consideration of hybridization and electron correlation effects. The obtained values of the spin magnetic moment by the cluster model analyses are in agreement with the results of the band structure calculation. The calculated result shows that the doped holes created by the Cr deficiency exist mainly in the Te 5*p* orbital of $Cr_{1-\delta}Te$, whereas the holes are likely to be in the Cr 3*d* state for Cr_5S_6.

DOI: 10.1103/PhysRevB.70.064402 PACS number(s): 71.28.+d

I. INTRODUCTION

Chromium chalcogenides $Cr_{1-\delta}X(X=S, Se, Te)$ with metal-deficient NiAs-type crystal structures show various magnetic and electronic properties.[1] Among them, chromium tellurides $Cr_{1-\delta}Te$ are ferromagnets with metallic conductivity with Curie temperatures of 170–360 K.

$Cr_{1-\delta}Te$ with $\delta<0.1$ form the hexagonal NiAs crystal structure, while Cr_3Te_4 ($\delta=0.25$) and Cr_2Te_3 ($\delta=0.33$) form monoclinic and trigonal crystal structures, where Cr vacancies occupy in every second metal layer.[2] The ordered magnetic moments evaluated from the magnetization measurements show much smaller values such as 2.4–2.7 μ_B for the $Cr_{1-\delta}Te$ with $\delta<0.1$, 2.35 μ_B for Cr_3Te_4 ($\delta=0.25$), and 2.0 μ_B for Cr_2Te_3 ($\delta=0.33$) than those expected from the ionic model.[3–14] According to neutron-diffraction studies, the small value of saturation magnetization is partly explained if we take the spin canting into account for $\delta=0.125$, 0.167, and 0.25.[10] The magnetic moment induced on the Cr ion for $\delta=0.25$ is close to an integral number of Bohr magnetons, suggesting the existence of mixed valence Cr.[10] However, for Cr_2Te_3 ($\delta=0.33$), the ordered magnetic moment of 2.65 −2.70 μ_B, deduced from the neutron diffraction is much smaller than that calculated using the ionic model 3 μ_B, suggesting the itinerant nature of the *d* electrons.[10,15]

Electronic specific heat coefficients γ are very dependent on δ. The estimated γ for Cr_5Te_6 ($\delta=0.167$), Cr_3Te_4 ($\delta=0.25$), and Cr_2Te_3 ($\delta=0.333$) are 10, 1, and 4 mJ/atom/K^2.[16] The γ for Cr_3Te_4 is quite close to the predicted value 1.0–1.4 mJ/atom/K^2 using the calculated density of states (DOS) at the Fermi level (E_F), while that for Cr_2Te_3 is much larger than the predicted one $\gamma\sim0.82$ −0.96 mJ/atom/K^2.[18,17] Such large γ values suggest that electron correlation effects are also important in Cr_5Te_6 and Cr_2Te_3. The electron correlation effects in these "itinerant ferromagnets" $Cr_{1-\delta}Te$ has been discussed with the photoemission spectra.[19] It has been pointed out that the spectral weight in $E_B=2-4$ eV observed in the photoemission spectra of $Cr_{0.95}Te$ and Cr_3Te_4 cannot be explained by the theoretical band structure calculation, and the intensity at E_F is found to be smaller than the theoretical DOS. On the other hand, the spectral weight in $E_B=2-4$ eV has been reproduced with the configuration interaction cluster-model calculation, indicating the importance of the electron correlation effect in $Cr_{1-\delta}Te$.[19]

In contrast to the telluride compounds, $Cr_{1-\delta}S$ shows an antiferromagnetic structure and some of them present a metal-semiconductor transition.[1] Among them, Cr_5S_6 shows a ferri-antiferromagnetic phase transition below 150 K. In the ferrimagnetic phase above 150 K, a tiny net magnetic moment appears as a result of the antiparallel spin alignment between the adjacent Cr atoms with slightly different magnetic moments.[20] Recently, in the analogy of the perovskite manganites, a collossal magnetoresistance has been found

for the sulfur deficient Cr_2S_3, which may contain both $Cr^{3+}(d^3)$ and $Cr^{2+}(d^4)$ ions.[21,22]

There has been a study of electronic structure using a band structure calculation to clarify the several magnetic and electronic properties depending on δ and the X atom of $Cr_{1-\delta}X(X=S, Se, Te)$.[18,23] The calculation has successfully described the antiferromagnetic ground state for CrS, whereas the ferromagnetic state has not been properly described for CrTe.[23]

Here we present a Cr $2p$ soft x-ray absorption (XAS) and x-ray magnetic circular dichroism (XMCD) spectra of ferromagnetic $Cr_{1-\delta}Te$ and ferrimagnetic Cr_5S_6. It is known that core XAS is a powerful tool to study the element specific valence electronic states of materials. XMCD in the core XAS spectrum provides us with useful information on the element specific spin and orbital magnetic moments with use of the "sum rule."[24–26] It is widely known that the spectral shapes of the XAS and XMCD spectra are strongly dependent on the electronic states or the electronic configuration of the derived atom. In addition, these line shapes can be remarkably affected by the intersite hybridization between the surrounding atoms or by the band structure of the crystal. In other words, the spectra can be a good fingerprint of the electronic states inside the crystals. For example, the valency (or the electron number) can be determined by the XAS and XMCD spectral line shapes. One can also determine several physical parameters such as the Coulomb repulsion energy, the charge transfer energy, as well as the hybridization energy from the analyses of experimental XAS and XMCD spectral line shapes. In order to understand how the electronic states are related to the δ and X atom dependences of the magnetic and electronic properties, we have performed Cr $2p$ XAS and XMCD experiments on $Cr_{1-\delta}Te$ and Cr_5S_6.

II. EXPERIMENTAL

Polycrystalline samples were synthesized from mixed powders of constituent elements. They were sealed in evacuated silica tubes, which were heated for a week at 1000 °C. After this, the samples were ground and sealed in silica tubes again and heated for 2 h at 1450 °C and then cooled gradually to 1000 °C and finally quenched into water.[28] The stoichiometry and the homogeneity of $Cr_{1-\delta}Te$ and Cr_5S_6 have been estimated by means of electron probe micro analysis (EPMA). X-ray diffraction studies confirmed that all of the samples were in a single phase.

Cr $2p$ core absorption spectroscopy (XAS) and x-ray magnetic circular dichroism spectra were measured at BL25SU of SPring-8 in Japan.[29–32] Circularly polarized light was supplied from a twin-helical undulator, with which almost 100% polarization was obtained at the peak of the first-harmonic radiation. After having set the two undulators to opposite helicity, helicity reversal was realized by closing one undulator and fully opening the other.[31] Cr $2p$ XAS spectra were measured by means of the total photoelectron yield method by directly detecting the sample drain current while changing the photon energy $h\nu$. The photon energy resolution was set to $E/\Delta E=5000$ for the Cr $2p$ core excitation regions. The measurement was performed in the Faraday geometry with both the incident light and the magnetization perpendicular to the sample surface. We used two pairs of permanent dipole magnets with holes for passing the excitation light. The external magnetic field of $\sim$1.4 T at the sample position was alternatingly applied by setting one of the two dipole magnets on the optical axis by means of a moter-driven linear feedthrough. The XMCD spectra were taken for a fixed helicity of light by reversing the applied magnetic field at each $h\nu$. In the present paper, the XMCD spectrum is defined as I_+-I_-, where I_+ and I_- represent the absorption spectra for the direction of magnitization (which is opposite to the direction of the majority spin) parallel and antiparallel to the photon helicity, respectively.[29] Clean surfaces were obtained by *in situ* scraping of the samples with a diamond file under ultrahigh vacuum condition (3×10^{-8} Pa). The cleanliness of the sample surfaces was first checked by the disappearance of a typical structure related to Cr oxides. We could also check the degree of contamination from the magnitude of the XMCD signal, because its amplitude grew and finally saturated when the sample surface became clean enough. We considered that the unscraped or contaminated surface was covered with antiferromagnetic or paramagnetic compounds such as Cr_2O_3, which hardly contribute to the XMCD spectrum. It is generally known that the the total photoelectron yield reflects the absorption spectrum in the core-excitation region. The temperatures during the measurement were $\sim$110 K for $Cr_{1-\delta}Te$ and 200 K for Cr_5S_6 (ferrimagnetic phase).

III. CI CLUSTER MODEL CALCULATION WITH FULL MULTIPLETS

The CI cluster model calculation has been done with a program code developed by Tanaka by means of the recursion method.[33] The detailed procedures are described elsewhere.[34] Slater integrals have been calculated by Cowan's code and the calculated values are listed in Table I. In the calculation, the Slater integrals are scaled down to 80% of the listed values to take into account intra-atomic relaxation effect.

IV. RESULTS AND DISCUSSION

The XAS and XMCD spectra in the Cr $2p$ core excitation region have been measured for $Cr_8Te_9(\delta=0.11)$, $Cr_5Te_6(\delta=0.17)$, $Cr_3Te_4(\delta=0.25)$, $Cr_2Te_3(\delta=0.33)$, and $Cr_5S_6(\delta=0.17)$. The Cr $2p$ XAS (I_+ and I_-) spectra with both helicities of incident radiation and the XMCD (I_+-I_-) spectra of Cr_5Te_6 are shown in Figs. 1(a) and 1(b). It is found that the $2p_{3/2}$ and the $2p_{1/2}$ core absorption peaks are located at about 576 and 585 eV, and the broad hump is found around the photon energy of 600–605 eV. Since the core level binding energies (E_B) of the Cr $2p$ and Te $3d$ levels are quite close to each other, one may expect the overlapping of these absorption edges.[35] We expect much lower Te $3d\rightarrow5p$ absorption cross section ($<5\%$) compared to that of the Mn $2p\rightarrow3d$ absorption as observed, i.e., in Te $4d\rightarrow5p$ absorption spectrum of $MnTe_2$.[36] We also expect that the observed Cr $2p$ XAS fine structures are almost unaffected by the Te $3d$ XAS

TABLE I. *Ab initio* Hartree-Fock values of the Slater integrals and spin-orbit coupling constants (in units of eV). In the actual calculation, the Slater integrals have been scaled to 80% of these values to take into account intra-atomic relaxation effect.

	configuration	$F^2(d,d)$	$F^4(d,d)$	$F^2(p,d)$	$G^1(p,d)$	$G^3(p,d)$	$\xi(3d)$	$\xi(2p)$
Cr	d^3	10.777	6.755				0.035	
	d^4	9.649	6.002				0.030	
	d^5	8.357	5.146				0.025	
	d^6	6.910	4.205				0.021	
	p^5d^4	11.596	7.270	6.526	4.788	2.722	0.047	5.667
	p^5d^5	10.522	6.552	5.841	4.204	2.388	0.041	5.668
	p^5d^6	9.303	5.738	5.151	3.644	2.069	0.035	5.669
	p^5d^7	7.867	4.801	4.461	3.155	1.768	0.030	5.671

spectrum because the Te 3*d* core absorption is expected to be very broad due to the wide conduction band derived from the itinerant natre of the Te 5*p* electrons. Therefore, one can assume that the Te 3*d* core absorption spectrum behaves as a background and the observed XAS spectra in the present photon energy range mostly reflect the Cr 2*p* core absorption. However, the broad hump at 600–605 eV can be still assigned to the Te $3d \rightarrow 5p$ absorption mainly because the observed XMCD asymmetry is negligible in this energy region. It is found that the intensity of I_+ is larger than that of I_- in the $2p_{3/2}$ core absorption region, whereas the intensity of I_+ is smaller than that of I_- in the $2p_{1/2}$ region. In addition, the spectral weight of I_+ is shifted to lower energy compared to I_- in both $2p_{3/2}$ and $2p_{1/2}$ regions. This derives the complicated XMCD ($I_+ - I_-$) structures as shown by the solid line in Fig. 1(b). Here, the spectrum (solid line) shows remarkable XMCD with positive sign at the $2p_{3/2}$ core absorption edge ($h\nu$=575.5 eV) as marked with A, which is followed by the smaller asymmetry with negative sign ($h\nu$=578 eV as represented by B. It is noticed that the XMCD signal does not reach zero even in the region between the spin-orbit split 2*p* components. There is still finite and negative XMCD on the lower-energy side of the $2p_{1/2}$ absorption edge ($h\nu$ =583 eV). Then one finds a small positive ($h\nu$=584 eV) and a large negative ($h\nu$=585.5 eV) XMCD peak with increasing $h\nu$ as marked with C, D, and E in Fig. 1(b). To eliminate the possible instrumental asymmetries, we have taken the spectra by reversing the helicity of the incident radiation. As a result of this procedure, it is found that the observed XMCD signals with opposite helicities of the incident lights are quite symmetric with respect to the zero line as shown by the solid and dashed line. This means that the observed complicated structures of the XMCD spectrum are intrinsic.

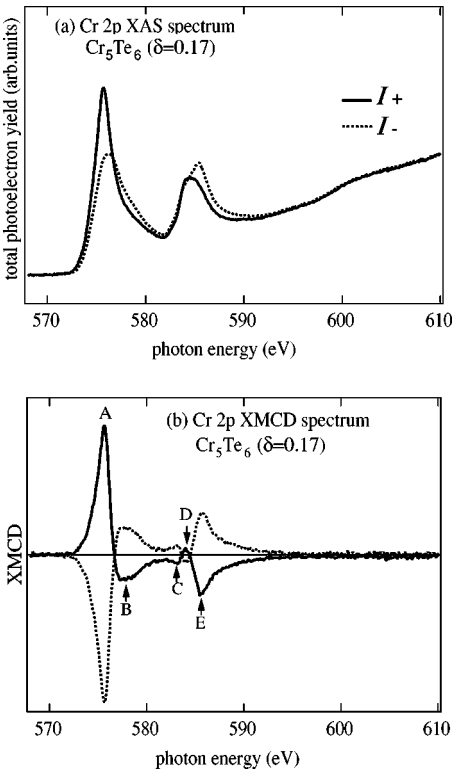

FIG. 1. (a) Cr 2*p* XAS spectra (I_+ and I_-) with different helicities of incident radiation. (b) XMCD spectrum ($I_+ - I_-$) of Cr_5Te_6 (solid line). The XMCD spectrum taken by reversing the helicity of the incident radiation is also shown (dashed line).

In Fig. 2, are shown the helicity averaged Cr 2*p* XAS spectra represented as $(I_+ + I_-)/2$ of (a) Cr_8Te_9(δ=0.11), (b) Cr_5Te_6(δ=0.17), (c) Cr_3Te_4(δ=0.25), (d) Cr_2Te_3(δ=0.33), and (e) Cr_5S_6(δ=0.17). In contrast to the spectrum of Cr_5Te_6 [Fig. 2(b)], a shoulder is found on the higher $h\nu$ side of the $2p_{3/2}$ edge in the spectrum of Cr_8Te_9. One also finds broad and small shoulder on the lower-energy side of the $2p_{1/2}$ peaks for δ=0.11. In the cases of $Cr_{1-\delta}Te$ with δ=0.17, 0.25 and 0.33, the linewidth of the $2p_{3/2}$ edge is narrower with some tail extending to the higher $h\nu$ compared to that for δ =0.11. In addition, the shoulder on the lower $h\nu$ side of the $2p_{1/2}$ edge has comparable spectral weight to that of the $2p_{1/2}$ main peak in these spectra. In addition, the broad humps are observed in the $h\nu$ region of 600–605 eV for all of the spectra as already pointed out for δ=0.17. The Cr 2*p* XAS spectrum of Cr_5S_6 shows a shoulder structure at the lower $h\nu$ of the $2p_{3/2}$ main peak, which is absent in the spectra of $Cr_{1-\delta}Te$ as shown in Fig. 2(e). Several structures are also found in the $2p_{1/2}$ energy region.

The XMCD spectra obtained as $I_+ - I_-$ of $Cr_{1-\delta}Te$ with δ =0.11, 0.17, 0.25, and 0.33 are shown in Fig. 3. We find that the overall line shape of the XMCD spectrum for δ=0.11 is similar to that for δ=0.17, in which all of the fundamental structures A–E are observed. This is not expected because

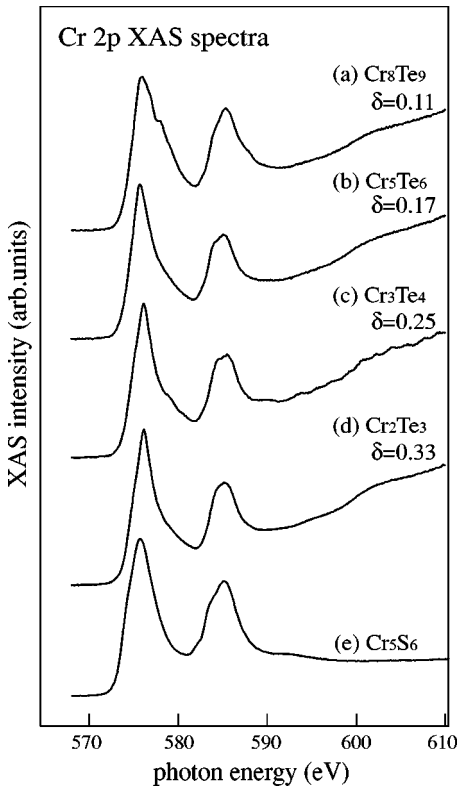

FIG. 2. Helicity averaged Cr $2p$ XAS spectra $(I_+ + I_-)/2$ of (a) Cr_8Te_9, (b) Cr_5Te_6, (c) Cr_3Te_4, (d) Cr_2Te_3, and (e) Cr_5S_6.

the XAS spectrum for $\delta = 0.11$ shows a different feature than that for $\delta = 0.17$ as stated above. Therefore we speculate that the shoulder structure at the $2p_{3/2}$ edge in the XAS spectrum for $\delta = 0.11$ [Fig. 2(a)] is extrinsic and might come from the remaining part of the chromium oxide in the sample, which hardly contribute to the XMCD spectrum because of its non-

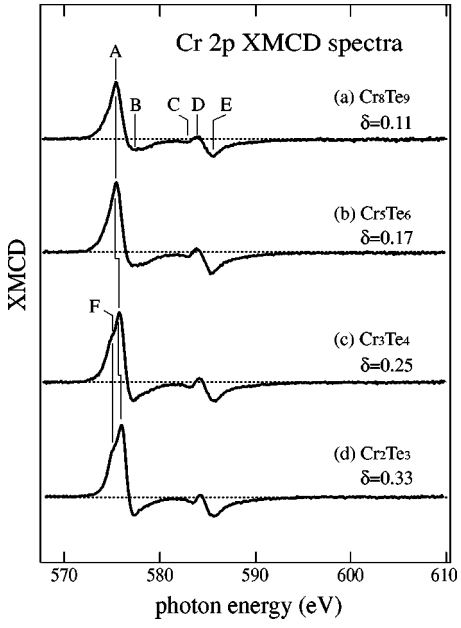

FIG. 3. Cr $2p$ XMCD $(I_+ - I_-)$ spectra (a) Cr_8Te_9, (b) Cr_5Te_6, (c) Cr_3Te_4, and (d) Cr_2Te_3.

ferromagnetic nature. For higher δ, we find that the XMCD spectrum for $\delta = 0.25$ resembles that for $\delta = 0.33$. It can be realized that the XMCD spectra for $\delta = 0.25$ and 0.33 show a different feature from those for $\delta = 0.11$ and 0.17, where the shoulder structure F is found on the low $h\nu$ side of the peak A and the negative structure B is sharper than those for $\delta = 0.11$ and 0.17 as shown in Fig. 3.

First, we have tried to evaluate the contribution of the orbital magnetic moment m_{orb} from the experimental XMCD spectra with the use of the following sum rule:[24,26]

$$m_{\mathrm{orb}} = \frac{4}{3}\frac{\int_{L_3+L_2}(I_+ - I_-)dh\nu}{\int_{L_3+L_2}(I_+ + I_-)dh\nu}(10 - n_d), \qquad (1)$$

where n_d represents $3d$ electron number. The estimated m_{orb} value is turned out to be almost negligible, suggesting the quenched Cr $3d$ orbital magnetic moment, in consistence with the measured g value $(g \sim 2)$.[6] A determination of the spin magnetic moment using sum rules for lighter transition metal elements such as Cr is questionable because the $2p_{3/2}$ and $2p_{1/2}$ edges are not well separated and are mixed with each other.[25,27] In this case, the best way to derive the spin magnetic moment m_{spin} is to fit the calculated spectrum to the experimental one as will be discussed below.

Next, in order to evaluate several parameters that control the physical properties of $Cr_{1-\delta}Te$, we have calculated the Cr $2p$ XAS and XMCD spectra by means of a configuration interaction (CI) cluster-model calculation with full multiplets assuming a $[CrTe_6]^{10-}$ cluster so as to reproduce the experimental spectra of $Cr_{1-\delta}Te$. Here, the nominal d electron numbers in Cr_8Te_9 ($\delta = 0.11$), Cr_5Te_6 ($\delta = 0.17$), Cr_3Te_4 ($\delta = 0.25$), and Cr_2Te_3 ($\delta = 0.33$) are ~ 3.75, 3.60, 3.33, and 3.00 per Cr atom, respectively, when we assume the Te valence to be $2-$. We have employed four charge-transfer states such as d^3, $d^4\underline{L}$, $d^5\underline{L}^2$, and $d^6\underline{L}^3$, where $\underline{L}$ denotes a hole in the Te $5p$ orbital. Thus the initial state is expanded by a linear combination of these four states and the final state is described by a linear combination of $\underline{2p}d^4$, $\underline{2p}d^5\underline{L}$, $\underline{2p}d^6\underline{L}^2$, and $\underline{2p}d^7\underline{L}^3$, where $\underline{2p}$ denotes a created hole in the $2p$ core level in the absorption final state. Slater integrals and spin-orbit coupling constants for d^3, d^4, d^5, and d^6 configurations in the initial state and for p^5d^4, p^5d^5, p^5d^6, and p^5d^7 in the XAS final states are listed in Table I. To perform the CI calculation, four adjustable parameters are introduced as follows; the charge-transfer energy $\Delta \equiv E(d^4\underline{L}) - E(d^3)$, the Coulomb interaction energy U_{dd} between the $3d$ electrons, the Coulomb attraction energy U_{cd} between the $2p$ core hole and $3d$ electron, the hybridization energy $V_{e_g}[=-\sqrt{3}(pd\sigma)]$ and the octahedral crystal field splitting $10Dq$. There has been a claim that a truncated basis set using at most two configurations $(d^n + d^{n+1}\underline{L})$ in the cluster model analysis would provide incorrect physical parameters especially for highly covalent materials with small Δ value that include a highly oxidized element (such as M^{3+} or M^{4+} if one compares it with the result using a complete basis set.[38] Here we use four basis set that should be enough to obtain reasonable physical param-

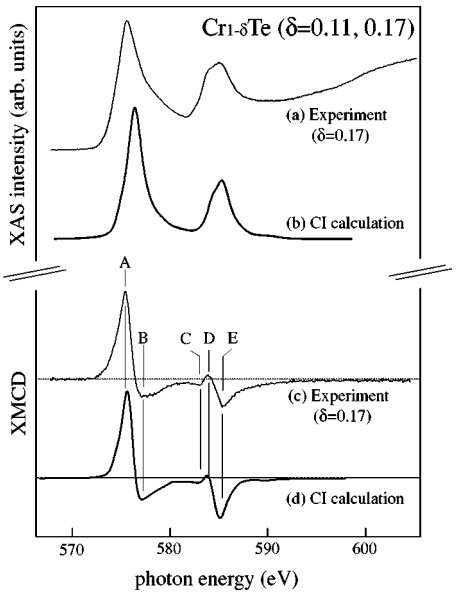

FIG. 4. (a), (c) The experimental Cr $2p$ XAS and XMCD spectra of Cr_5Te_6 ($\delta=0.17$) (thin solid lines). (b), (d) The calculated XAS and XMCD spectra by the CI cluster model with full multiplets of $[CrTe_6]^{10-}$ cluster (thick solid lines).

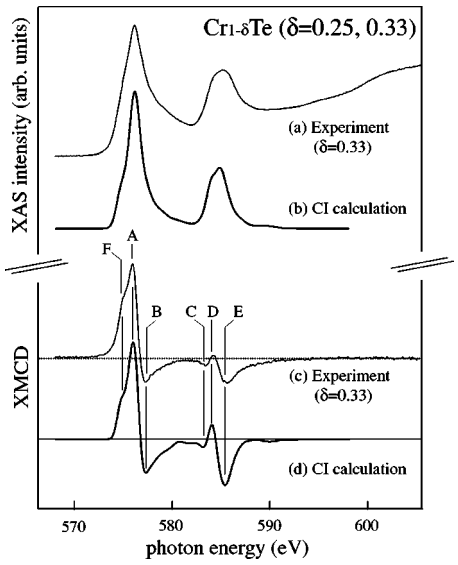

FIG. 5. (a), (c) The experimental Cr $2p$ XAS and XMCD spectra of Cr_2Te_3 ($\delta=0.33$) (thin solid lines). (b), (d) The calculated XAS and XMCD spectra by the CI cluster model with full multiplets of $[CrTe_6]^{10-}$ cluster (thick solid lines).

eters, which would be confirmed from the result that the state with highest order ($=d^6\underline{L}^3$) is found to show very small weight ($<7\%$).

We have used the $U_{dd}\sim 2.3$ eV, which has been estimated from the Cr $M_{23}VV$ Auger-electron spectra and the self-convolution of the Cr $3d$-derived spectra.[19] The same value of $V_{e_g}=1.3$ eV [$(pd\sigma)=-0.75$ eV] has been considered, where it has been evaluated by using the formula $(pd\sigma)=\eta_{pd\sigma}(\hbar^2/m)(r_d^{1.5}/d^{3.5})$ with $\eta_{pd\sigma}=-2.95$ and $r_d(\mathrm{Cr})=0.9$ Å.[37] Here, U_{cd} has been fixed to $U_{dd}/U_{cd}=0.83$ and the relationship $(pd\sigma)/(pd\pi)=-2.0$ has been assumed.

For $Cr_{1-\delta}Te$ with $\delta=0.11$ and 0.17, we have adjusted the charge transfer energy Δ and $10Dq$ to fit the experimental XAS and XMCD spectra. Figure 4(b) and 4(d) show the calculated XAS and XMCD spectra with $\Delta=-2.0$ eV and $10Dq=0.7$ eV, which are broadened by the Lorenzian and Gaussian functions with the FWHM of 0.6 eV for each. It is noticed that the calculated XAS spectrum fits well with the experimental spectra for $\delta=0.11$ and 0.17 including the shoulder structure in the $2p_{1/2}$ region. The calculated XMCD spectrum reproduces not only the dispersive XMCD feature at the $2p_{3/2}$ edge (A and B), but also the structures at $2p_{1/2}$ edge including the small positive structure found in the lower $h\nu$ region (C, D, and E) as shown in Fig. 4(d). It is noted here that we have obtained the negative value of Δ, which means that the ground state is not dominated by the d^3 state but by the $d^4\underline{L}$ and $d^5\underline{L}^2$ states because the energy differences $E(d^4\underline{L})-E(d^3)$ and $E(d^5\underline{L}^2)-E(d^3)$ are expressed as $\Delta(=-2.0$ eV) and $2\Delta+U_{dd}(=-1.7$ eV), respectively, when the hybridization (V_{e_g}) is off. That is, the most stable $d^4\underline{L}$ state is formed by the charge transfer from the ligand Te $5p$ orbitals to the Cr $3d$ orbitals. The calculated result also shows that the weight of $d^4\underline{L}+d^5\underline{L}^2$ exceeds 80%, which is due to the strong hybridization between Cr $3d$ and Te $5p$ orbitals. The averaged $3d$ electron number n_d is 4.5, which is much larger than 4 (Cr^{2+}) as shown in Table II. The estimated m_{spin} and m_{orb} are 3.6 μ_B and -0.02 μ_B, respectively. Such a quite small m_{orb} stems from the dominant $d^5\underline{L}^2$ configuration in the ground state and is consistent with the negligible value with use of the sum rule as mentioned above. The calculated $m_{\mathrm{spin}}=3.6$ μ_B is consistent with the values given by the band-structure calculation 3.3 μ_B (Ref. 18) but is much larger than the saturation magnetic moment ~ 2.5 μ_B.

We have also applied the calculation to $Cr_{1-\delta}Te$ with $\delta=0.25$ and 0.33. Figures 5(b) and 5(d) show the calculated XAS and XMCD spectra with the parameters $\Delta=-1.5$ eV and $10Dq=1.0$ eV. We find a good correspondence between the calculated XAS/XMCD spectra and the experimental ones. We recognize that the calculated XMCD spectrum not only reproduces the observed fundamental structures A–E

TABLE II. Parameters obtained from the analyses of the XAS and XMCD spectra of Cr_8Te_9 and Cr_2Te_3 with CI cluster model calculation (in units of eV). We assumed $U_{dd}/U_{cd}=0.83$ and $(pd\sigma)/(pd\pi)=-2$.

	Δ	$10Dq$	U_{dd}	$pd\sigma$	n_d	m_{spin}	m_{orb}
$Cr_{1-\delta}Te(\delta=0.11,0.17)$	−2.0	0.7	2.3	−0.75	4.5	3.6	−0.02
$Cr_{1-\delta}Te(\delta=0.25,0.33)$	−1.5	1.0	2.3	−0.75	4.3	3.2	−0.03
Cr_5S_6	0.5	1.0	3.1	−0.87	3.8	3.1	−0.05

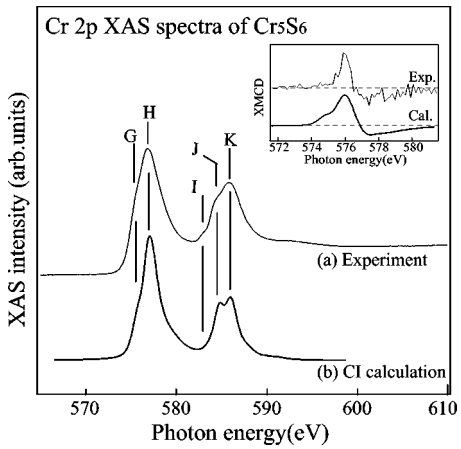

FIG. 6. (a) Helicity averaged Cr $2p$ XAS spectrum $(I_+ + I_-)/2$ of Cr_5S_6 (thin solid lines). (b) The calculated XAS spectrum by the CI cluster model of $[CrS_6]^{10-}$ cluster (thick solid lines). The inset shows the experimental (top) and the calculated (bottom) spectra with the sama parameter set as used for the XAS spectrum.

but also the shoulder F as shown in Figs. 5(c) and 5(d). It should be remarked here that a little bit larger $10Dq$ (=1.0 eV) value compared to that for $\delta=0.11$ and 0.17 ($10Dq=0.7$ eV) introduced the shoulder F in the XMCD spectra for $\delta=0.25$ and 0.33. From this result, n_d is found to be 4.2 and the calculated m_{spin} and m_{orb} are estimated to be 3.2 μ_B and -0.03 μ_B, respectively, as listed in Table II. We find again that the small m_{orb} is consistent with the XMCD result. The present n_d and m_{spin} are smaller than that for $\delta=0.11$ and 0.17. It is noted that the value of m_{spin} is comparable to that obtained by the band structure calculation ($\sim$3.3 for both $\delta=0.25$ and 0.33),[18] but is larger than the saturation magnetic moment of $\sim 2.0-2.7$ μ_B.

Finally the calculated results for Cr_5S_6 are shown here. We have evaluated the value $V_{e_g}=1.5$ eV $[(pd\sigma)=-0.87$ eV] using the same formula as used for the telluride. It can be understood that the larger value for the sulfide is due to the reduced Cr-X atomic distance, where Cr-S and Cr-Te atomic distances evaluated by the x-ray powder diffraction are 2.4 and 2.8 Å, respectively. We have adjusted the parameters so as to fit the observed energy splitting of 1.2 eV between G and H at the $2p_{3/2}$ component and of 1.4 eV between J and K at the $2p_{1/2}$ component as shown in Fig. 6. The obtained parameters are $\Delta=0.5$ eV, $U_{dd}=3.1$ eV, and $10Dq=1.0$ eV. The value of $U_{dd}=3.1$ eV is consistent with the recent photoemission and inverse photoemission experiment by Koyama *et al.*, where the energy splitting between the phtoemission and inverse photoemission spectra is $\sim$3.0 eV.[39] It is noticed that the XMCD spectrum of Cr_5S_6 in the ferrimagnetic phase has been reproduced with the same parameter set as shown in the inset of Fig. 6, where the observed plus-minus feature is recognized in the calculation. The obtained positive Δ value for Cr_5S_6 is reasonable instead of the negative Δ for $Cr_{1-\delta}Te$ because of the larger electron negativity of S than Te, which would be further confirmed by the reported larger value of $\Delta=5.2$ eV for Cr_2O_3.[40] In Cr_5S_6, the d^3 and $d^4\underline{L}$ states dominate the ground state, in contrast to the tellurides. The evaluated average electron number n_d is found to be 3.8, which is smaller than that of the telluride with the same stoichiometry.

We have obtained the similar parameter values of Δ and $10Dq$ for $Cr_{1-\delta}Te$ with $\delta=0.11-0.33$, which indicates that the local Cr $3d$ electronic states are not much affected by the Cr deficiency δ. This feature is really explained by the obtained negative value of Δ, where the lowest-energy state can be described as $d^4\underline{L}$. Thus we interpret that the doped holes created by the Cr deficiency do not stay in the Cr $3d$ states but exist in the Te $5p$ orbitals for $Cr_{1-\delta}Te$. This is consistent with the calculated band structure of $Cr_{1-\delta}Te$, where the hole pocket derived from the Te $5p$ state appears around Γ point in the Brillouin zone when the Cr vacancy is introduced in the material.[18] In contrast, the positive Δ value for Cr_5S_6 leads to the lowest-energy state of d^3, which means the doped holes are likely to be in the Cr $3d$ orbitals. This interpretation is consistent with the ferrimagnetic resonance experiment on Cr_5S_6, where the electron hopping between the Cr^{2+} and Cr^{3+} ions is suggested.[41]

V. CONCLUSION

We have observed the Cr $2p$ XAS and XMCD spectra of Cr_8Te_9 ($\delta=0.11$), Cr_5Te_6 ($\delta=0.17$), Cr_3Te_4 ($\delta=0.25$), Cr_2Te_3 ($\delta=0.33$), and Cr_5S_6. The observed changes with the Cr vacancy in the experimental XMCD spectra of $Cr_{1-\delta}Te$ are found to be small. The experimental XAS and XMCD spectra of $Cr_{1-\delta}Te$ have been compared with the result of the CI cluster-model calculation. We have obtained the best-fit parameter values $\Delta=-2.0$ eV, $10Dq=0.7$ eV for $\delta=0.11$ and 0.17 and $\Delta=-1.5$ eV and $10Dq=1.0$ eV for $\delta=0.25$ and 0.33 with $U_{dd}=2.3$ eV and $V_{e_g}=1.3$ eV fixed for all of $Cr_{1-\delta}Te$ studied. Both the experiment and the calculation give a quenched Cr $3d$ orbital magnetic moment for $Cr_{1-\delta}Te$, in agreement with the observed g value. The obtained values of the spin magnetic moment by the cluster model analyses are consistent with the results of the band structure calculation. In contrast to these negative Δ values for the tellurides, we have found the positive $\Delta(=0.5$ eV) for Cr_5S_6. It is concluded from these results that the doped holes created by the Cr deficiency exist mainly in the Te $5p$ orbitals for $Cr_{1-\delta}Te$, whereas the holes are likely to be in Cr $3d$ state for Cr_5S_6. This interpretation for $Cr_{1-\delta}Te$ is consistent with the unchanged feature of the XMCD spectrum with the Cr defect concentration δ and the band structure calculation.

ACKNOWLEDGMENTS

The authors would like to thank Dr. Y. Saitoh of the Japan Atomic Energy Research Institute for a fine adjustment of the monochromator and Professor A. Fujimori of the University of Tokyo and Professor T. Kanomata of Tohoku Gakuin University for their fruitful discussion. This work was done under the approval of the SPring-8 Advisory Committee (Proposal No. 2000B0439-NS -np). This work was supported by the Ministry of Education, Culture, Sports, Science and Technology.

*Electronic address: akiok@hiroshima-u.ac.jp

[1] K. Adachi and S. Ogawa, *Magnetic Properties of Non-Metals*, in Landölt-Bornstein New Series, Vol. III/27a, edited by H. P. J. Wijn (Springer, Berlin, 1988), p. 99.
[2] H. Ipser and K. L. Komarek, J. Less-Common Met. **92**, 265 (1983).
[3] F. K. Lotgering and E. W. Gorter, J. Phys. Chem. Solids **3**, 328 (1957).
[4] T. Hirone and S. Chiba, J. Phys. Soc. Jpn. **15**, 1991 (1960).
[5] A. Ohsawa, Y. Yamaguchi, N. Kazama, H. Yamaguchi, and H. Watanabe, J. Phys. Soc. Jpn. **33**, 1303 (1972).
[6] N. P. Grazhdankina and R. I. Zainullina, Zh. Eksp. Teor. Fiz. **59**, 1896 (1970) [Sov. Phys. JETP **32**, 1025 (1971)].
[7] T. Hashimoto and M. Yamaguchi, J. Phys. Soc. Jpn. **27**, 1121 (1969).
[8] M. Yamaguchi and T. Hashimoto, J. Phys. Soc. Jpn. **32**, 635 (1972).
[9] A. F. Andresen, Acta Chem. Scand. (1947-1973) **17**, 1335 (1963).
[10] A. F. Andresen, Acta Chem. Scand. (1947-1973) **24**, 3495 (1970).
[11] T. Hashimoto, K. Hoya, M. Yamaguchi, and I. Ichitsubo, J. Phys. Soc. Jpn. **31**, 679 (1971).
[12] T. Kanomata, Y. Sugawara, T. Kaneko, K. Kamishima, H. Aruga Katori, and T. Goto, J. Alloys Compd. **297**, 5 (2000).
[13] S. Ohta, T. Kanomata, T. Kaneko, and H. Yoshida, J. Phys.: Condens. Matter **5**, 2759 (1993).
[14] T. Kanomata, Y. Sugawara, K. Kamishima, H. Mitamura, T. Goto, S. Ohta, and T. Kaneko, J. Magn. Magn. Mater. **70**, 223 (1987).
[15] T. Hamasaki, T. Hashimoto, Y. Yamaguchi, and H. Watanabe, Solid State Commun. **16**, 895 (1975).
[16] F. Grønvold and E. F. Westrum, Jr., Z. Anorg. Allg. Chem. **328**, 272 (1964).
[17] S. Ishida and S. Asano (unpublished).
[18] J. Dijikstra, H. H. Weitering, C. F. van Bruggen, C. Haas, and R. A. de Groot, J. Phys.: Condens. Matter **1**, 9141 (1989).
[19] K. Shimada, T. Saitoh, H. Namatame, A. Fujimori, S. Ishida, S. Asano, M. Matoba, and S. Anzai, Phys. Rev. B **53**, 7673 (1996).
[20] Van Larr, Phys. Rev. **156**, 654 (1967).
[21] J. M. D. Coey, M. Viret, and S. von Molnar, Adv. Phys. **48**, 167 (1999).
[22] P. Vaqueiro, A. V. Powell, A. I. Coldea, C. A. Steer, I. M. Marshall, S. J. Blundell, J. Singleton, and T. Ohtani, Phys. Rev. B **64**, 132402 (2001).
[23] J. Dijikstra, C. F. van Bruggen, C. Haas, and R. A. de Groot, J. Phys.: Condens. Matter **1**, 9163 (1989).
[24] B. T. Thole, P. Carra, F. Sette, and G. van der Laan, Phys. Rev. Lett. **68**, 1943 (1992).
[25] P. Carra, B. T. Thole, M. Altarelli, and X. Wang, Phys. Rev. Lett. **70**, 694 (1993).
[26] C. T. Chen, Y. U. Idzerda, H.-J. Lin, N. V. Smith, G. Meigs, E. Chaban, G. H. Ho, E. Pellegrin, and F. Sette, Phys. Rev. Lett. **75**, 152 (1995).
[27] Y. Teramura, A. Tanaka, and T. Jo, J. Phys. Soc. Jpn. **65**, 1053 (1996).
[28] M. Koyama, H. Sato, M. Taniguchi, and Y. Ueda (unpublished).
[29] S. Suga, S. Imada, A. Yamasaki, S. Ueda, T. Muro, and Y. Saitoh, J. Magn. Magn. Mater. **233**, 60 (2001).
[30] S. Suga, Nucl. Instrum. Methods Phys. Res. A **467–468**, 1388 (2001).
[31] Y. Saitoh, H. Kimura, Y. Suzuki, T. Nakatani, T. Matsushita, T. Muro, T. Miyahara, M. Fujisawa, K. Soda, S. Ueda, H. Harada, M. Kotsugi, A. Sekiyama, and S. Suga, Rev. Sci. Instrum. **71**, 3254 (2000).
[32] Y. Saitoh, H. Kimura, Y. Suzuki, T. Nakatani, T. Matsushita, T. Muro, T. Miyahara, M. Fujisawa, K. Soda, S. Ueda, A. Sekiyama, S. Imada, and S. Suga, Nucl. Instrum. Methods Phys. Res. A **467–468**, 553 (2001).
[33] V. Heine, *Solid State Physics*, edited by H. Ehrenreich, F. Seitz, and D. Turnbull (Academic Press, New York, 1980), Vol. 35, p. 87.
[34] A. Tanaka and T. Jo, J. Phys. Soc. Jpn. **63**, 2788 (1994).
[35] J. C. Fuggle and N. Martensson, J. Electron Spectrosc. Relat. Phenom. **21**, 275 (1980). The binding energies of Cr $2p_{3/2}$ and $2p_{1/2}$ are 583.8 and 574.1 eV, while those of Te $3d_{5/2}$ and $3d_{3/2}$ are 583.4 and 573 eV.
[36] K. V. Kaznacheyev, T. Muro, T. Matsushita, T. Iwasaki, Y. Kuwata, H. Harada, S. Suga, H. Ishii, T. Miyahara, T. Mizokawa, A. Fujimori, T. Harada, and T. Kanomata, Phys. Rev. B **58**, 13 491 (1998). The integrated XAS intensity ratio of Te4*d*/Mn3*p* is roughly estimated to be 10%, which should be scaled to about 50% because of the one-to-one composition in CrTe instead of the one-to-two concentration in $MnTe_2$. Here we assume that the Mn3*p*/Te4*p* absorption cross section ratio is comparable to that of the Cr2*p*/Te3*p*.
[37] W. A. Harrison, *Electronic Structure and the Physical Properties of Solids* (Dover, New York, 1989).
[38] P. Mahadevan and D. D. Sarma, Phys. Rev. B **61**, 7402 (2000).
[39] M. Koyama, H. Sato, Y. Ueda, C. Hirai, and M. Taniguchi, Solid State Commun. **125**, 243 (2003).
[40] A. E. Bocquet, T. Mizokawa, K. Morikawa, A. Fujimori, S. R. Barman, K. Maiti, D. D. Sarma, Y. Tokura, and M. Onoda, Phys. Rev. B **53**, 1161 (1996).
[41] H. Konno and M. Yuzuri, J. Phys. Soc. Jpn. **57**, 621 (1988).